Chemical Science

ROYAL SOCIETY OF CHEMISTRY

EDGE ARTICLE

View Article Online
View Journal

Cite this: DOI: 10.1039/d6sc01132b

All publication charges for this article have been paid for by the Royal Society of Chemistry

A dual-responsive cationic acridinium nanohoop: redox activity and acid/base-controlled reversible guest capture and release

Jiao Ming,[a] Jin Zhang,[b] Yan Hu,[a] Kai Lan,[a] Dongmei Zhang,[a] Ping Li,[a] Jiarong Miao,[a] Jiyong Jiang,[a] Xiaobo Zhang,[a] Hanchi Zhong,[a] Peiyuan Yu *[b] and Chuyang Cheng *[a]

Received 9th February 2026
Accepted 12th April 2026

DOI: 10.1039/d6sc01132b

rsc.li/chemical-science

In this work, we report a fully conjugated, radially cationic nitrogen-doped cycloparaphenylene derivative, **Ad[10]CPP$^+$**, constructed using the acridinium moiety as a functional building block. This compound exhibits remarkable reversibility in structural transformations under chemical stimuli and tunable redox behavior under electrochemical stimuli. Cyclic voltammetry reveals that **Ad[10]CPP$^+$** possesses multiple oxidation states and demonstrates significant redox versatility. Furthermore, **Ad[10]CPP$^+$** can reversibly transform from a near-circular configuration to a water-droplet shape upon hydroxide attack on the acridinium moiety when the acid concentration is lowered. The host–guest interaction between fullerene (C_{60}) and **Ad[10]CPP$^+$** was confirmed by NMR spectroscopy and single-crystal X-ray diffraction. Significantly, the host–guest system exhibits excellent fatigue resistance, enabling at least five consecutive cycles of chemically triggered fullerene capture and release through reversible structural transformations.

Introduction

Cycloparaphenylenes (CPPs), aromatic macrocycles composed of *para*-phenylene units, have garnered considerable attention since their first synthesis.[1–8] The interest is primarily attributed to their inherent ring strain[9–15] and unique radial cyclic π-conjugated architectures.[16–21] Over the past decade, the field has witnessed remarkable progress, as evidenced by the successful synthesis of CPPs and their derivatives of varying sizes.[22–28] Despite these advancements, the incorporation of heteroatoms, particularly nitrogen, remains underexplored.[8] Replacing phenylene units with nitrogen-containing aromatic rings can endow CPPs with acid–base responsiveness,[29] metal coordination capabilities,[30] and synthetic handles for constructing mechanically interlocked molecules.[31–33] Subsequent alkylation of these nitrogen atoms can convert the neutral macrocycles into cationic ones, introducing redox activity.[34,35] Both the amount and position of nitrogen doping can effectively modulate the photophysical[36] and supramolecular properties of CPPs.[37] Notably, in most reported cases, nitrogen atoms are incorporated at lateral positions of the CPP skeleton (Scheme 1a, left), as this approach aligns with conventional synthetic routes. In contrast, the direct fusion of nitrogen at the phenylene linkage sites, namely, axial doping, is far less common.[38–42] Such a configuration is predicted to markedly influence the nanoring's photophysical profile, introduce multiple accessible redox states,[38] and create a cavity with tunable size.[39] However, the limited examples of axially *N*-doped carbon nanorings reported to date are, strictly speaking, not fully conjugated CPPs. Recently, we reported the first fully conjugated cationic CPPs bearing pyridinium units at the phenylene linkages[43] (Scheme 1a, right), a long-standing synthetic challenge due to ring strain and cation instability under basic conditions. This synthetic challenge was effectively overcome by introducing an *N*-phenylpiperidine derivative strain-release unit followed by aromatization to construct a pyridinium moiety. In the present work, we extend this design by employing a π-expanded motif, in the form of an acridine fragment, as a strain-release unit. This approach not only enhances synthetic accessibility but also unlocks distinct functional advances. Specifically, we demonstrate that installing cationic nitrogen at the phenylene linkage sites in the form of acridinium enables reversible, stimuli-responsive switching of the macrocyclic framework between configurations in response to electrochemical and acid–base stimuli. This structural dynamism, in turn, facilitates controlled capture and release of guest molecules, advancing CPPs toward adaptive host–guest systems.

The rigid and curved conjugated structures of CPPs serve as ideal host molecules for fullerenes.[44–50] Their complementary shape and size facilitate strong π–π interactions with fullerenes, achieving binding constants of 10^5–10^6 M^{-1}. The rigid and strained macrocyclic constitution, however, also poses a challenge for incorporating reversible guest capture and release

[a]Key Laboratory of Green Chemistry & Technology, Sichuan University, Chengdu, 610064, China. E-mail: cycheng@scu.edu.cn

[b]Department of Chemistry, Guangming Advanced Research Institute, Southern University of Science and Technology, Shenzhen, 518055, China. E-mail: yupy@sustech.edu.cn

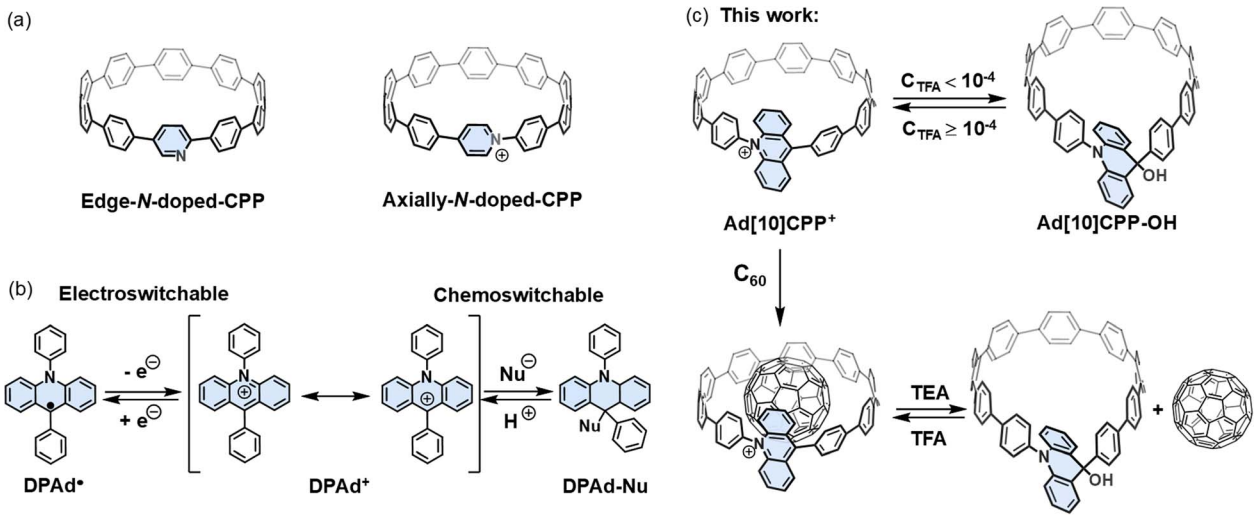

Scheme 1 Design concept of an acridinium functionalized CPP. (a) Edge-*N*-doped CPP and axially-*N*-CPP. (b) Reversible structural transformation of **DPAd$^+$** under electrochemical and chemical stimuli. (c) Reversible structural transformation and guest capture/release of **Ad[10]CPP$^+$** under chemical stimuli in this work.

functionality. Introducing stimuli-responsive motifs that can reversibly modulate the strained framework offers an effective strategy for achieving controlled guest capture and release. While several studies have incorporated stimuli-responsive motifs into CPPs to modulate the geometry of the strained macrocycle,[16,51–54] to the best of our knowledge, no examples of stimuli-responsive guest capture and release for CPPs have been reported thus far.

The acridinium unit is known for its reversible structural transformation in response to electrochemical and chemical stimuli.[55–63] Specifically, 9,10-diphenylacridinium (**DPAd$^+$**) is highly susceptible to nucleophilic attack and can reversibly transition between its radical state and cationic form under electrochemical control (Scheme 1b). In this study, we incorporate a **DPAd$^+$** fragment into the CPP skeleton to construct a functionalized strain macrocycle similar in size to **[10]CPP**, namely, **Ad[10]CPP$^+$** (Scheme 1c). We carried out a comprehensive investigation into the synthesis and structural, optical, electronic, and computational properties of **Ad[10]CPP$^+$**. Our findings revealed that **Ad[10]CPP$^+$** undergoes reversible structural transformations under electrochemical and acid/base stimulation. Furthermore, we performed extensive studies on the host–guest chemistry of **Ad[10]CPP$^+$** and successfully obtained the solid-state suprastructure of C_{60} captured by **Ad[10]CPP$^+$**. Most notably, **Ad[10]CPP$^+$** demonstrated the ability to bind and release C_{60} in response to acid/base stimuli, exhibiting excellent fatigue resistance over multiple cycles. This approach offers significant potential for expanding the applications of CPPs in supramolecular chemistry and materials science.

Results and discussion

Synthesis and structure characterization

The synthesis of the target molecule commenced with a macrocyclization step through a double-site Suzuki–Miyaura cross-coupling reaction between the bent dibromoacridine derivative **3** and the C-shaped diboronate[15,64] **7** (Fig. 1a). Our initial strategy anticipated that the $SnCl_2$-mediated reductive aromatization[65] would yield the desired acridinium product. However, the compound obtained did not align with our expectations; the ^{1}H NMR spectrum exhibited an unanticipated signal at 5.32 ppm, devoid of the characteristic deshielded aromatic signals above 8 ppm (Fig. 2a and S8). Moreover, the mass spectrometry data deviated by approximately one unit (Fig. S21). Single-crystal X-ray diffraction analysis ultimately confirmed that the product was a macrocycle with the acridinium unit hydrogenated (**Ad[10]CPP-H**), featuring an sp^3-hybridized carbon within the acridine moiety, which imparted a teardrop shape to the macrocycle with dimensions of 16.7 Å along the long axis and 11.0 Å along the short axis (Fig. 1b). The over-reduction, while not the desired outcome, was not detrimental, as the product remained a macrocycle with a structure closely resembling that of our target. Subsequently, we endeavored to oxidize **Ad[10]CPP-H** using 2,3-dichloro-5,6-dicyano-1,4-benzoquinone (DDQ) to achieve the acridinium macrocycle. Despite our efforts, the product again closely resembled the expected macrocycle but exhibited an additional signal at 2.86 ppm in the ^{1}H NMR spectrum, with the mass data offset by around 17 units (Fig. 2b, S11 and S22). Single-crystal X-ray diffraction revealed a macrocycle of similar teardrop shape (**Ad[10]CPP-OH**), with the only difference being the oxidation of a C–H bond to a C–OH group compared with **Ad[10]CPP-H** (Fig. 1c).

With the macrocycle in the anticipated oxidative state, we proceeded to acidify the sample using HBF_4 to protonate the hydroxy group and induce dehydration, aiming to convert the macrocycle into the cationic acridinium-functionalized final product (**Ad[10]CPP·BF$_4$**). The ^{1}H NMR spectrum demonstrated a complete transformation from **Ad[10]CPP-OH** to a new species, with the characteristic deshielded aromatic signal for

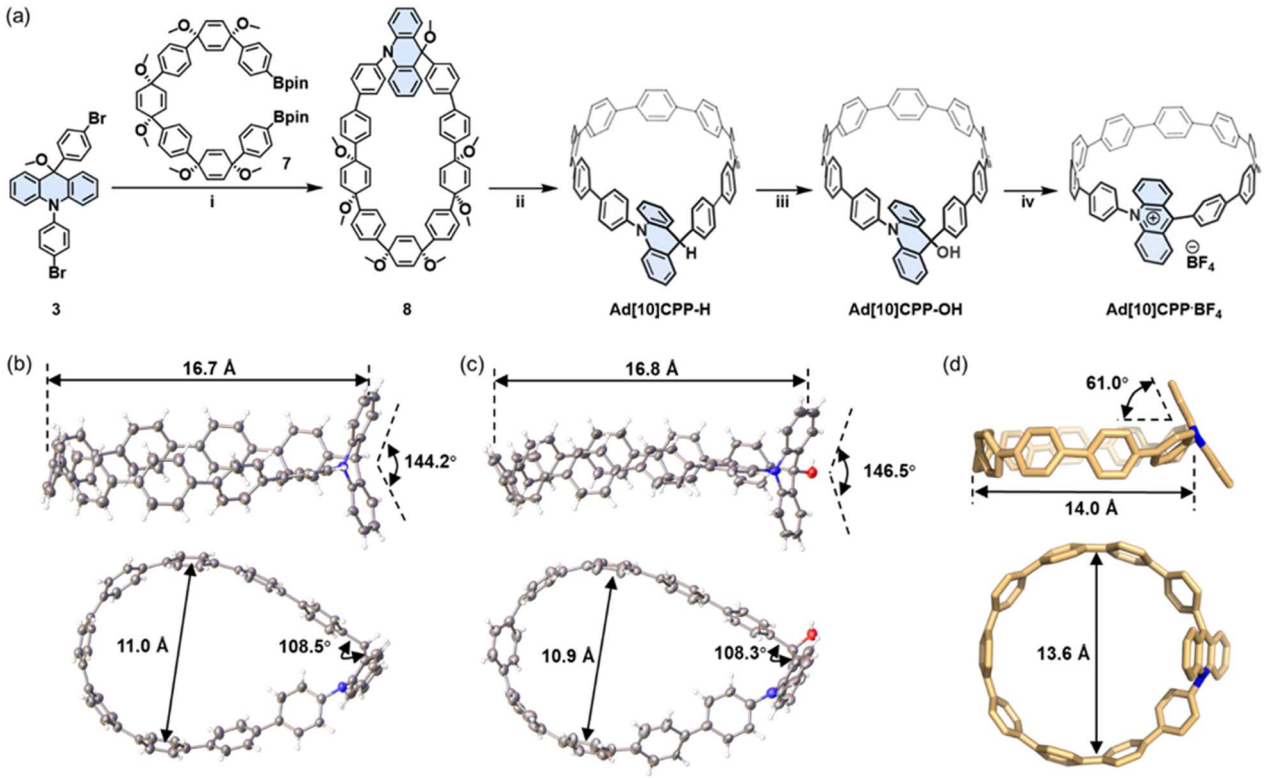

Fig. 1 (a) The synthetic route of **Ad[10]CPP·BF$_4$**. Reaction conditions: (i) $Pd(PPh_3)_4$, $NaHCO_3$, *n*-Bu_4NBr, toluene/methanol/H_2O, 90 °C, 24 h. (ii) $SnCl_2 \cdot 2H_2O$, concentrated HCl, THF, rt, 12 h, 13% over two steps. (iii) DDQ, CH_2Cl_2, rt, 12 h, 54%. (iv) HBF_4 (40% aq), CH_2Cl_2, rt, 3 h, quantitative by NMR. The ORTEP drawing of X-ray solid-state structures of (b) **Ad[10]CPP-H** and (c) **Ad[10]CPP-OH**. Thermal ellipsoids are set at 30% probability. Grey C, white H, blue N, and red O. Solvent molecules are omitted for clarity. For crystallographic details and CCDC numbers see the SI. (d) The DFT optimized geometry of the **Ad[10]CPP$^+$** cation (at the B3LYP-D3(BJ)/def2-SVP level). Color code: C yellow, N blue, O red and H white. Other hydrogen atoms, solvent molecules and counter ions are omitted for the sake of clarity.

H_a at 8.30 ppm and H_c at 7.99 ppm (Fig. 2c and S15). The high resolution MALDI-TOF MS spectrum confirmed the expected molecular weight of the acridinium macrocyclic cation (Fig. S23), thereby validating the successful synthesis of the desired macrocycle. **Ad[10]CPP·TFA** is also obtained by treating **Ad[10]CPP-OH** with excess trifluoracetic acid (TFA). The isolation of a solid **Ad[10]CPP·BF$_4$** or **Ad[10]CPP·TFA** sample proved to be elusive despite extensive efforts, attributed to the intrinsic instability of the cationic macrocycle under neutral conditions. Specifically, the acridinium moiety is highly vulnerable to nucleophilic attack, readily reverting to **Ad[10]CPP-OH** upon exposure to moisture. A TFA titration experiment revealed that the interconversion between **Ad[10]CPP$^+$** and **Ad[10]CPP-OH** occurs within the TFA range between 1.0×10^{-4} and 1.0×10^{-5} M in CH_2Cl_2 (Fig. S26). This highlights the dependency of the thermodynamic stability of the cationic macrocycle on acidic conditions. Strain energy calculations revealed a significant increase from 38.7 kcal mol^{-1} for **Ad[10]CPP-OH** to 56.2 kcal mol^{-1} for **Ad[10]CPP$^+$**. This substantial increase in ring strain imposes a considerable thermodynamic penalty, thereby disfavoring the formation of the cationic species (Fig. S73 and Table S5). Furthermore, the instability also hinders the crystal growth of the cationic macrocycle. Specifically, the gradual evaporation of the volatile acid (*e.g.*, TFA), which is essential for maintaining the cationic state, prevented the growth of diffraction-quality crystals over time. Despite months of dedicated efforts, including crystallization attempts in a nitrogen-filled glovebox, we were unable to obtain a single crystal suitable for X-ray diffraction analysis. Consequently, we employed density functional theory (DFT) calculations at the B3LYP-D3(BJ)/def2-SVP level to elucidate the structural characteristics of the acridinium macrocycle. The computational results depicted an elliptical nanoring with a long axis of 14.0 Å and a short axis of 13.6 Å. The acridinium aromatic plane is oriented at an angle of 61.0° relative to the macrocyclic plane (Fig. 1d). The torsion angles between the acridinium unit and its adjacent phenylene moieties were measured to be 51.5° and 67.3°, respectively. These values are notably larger than those between other phenylene rings (22.1° to 36.5°), a difference attributed to the steric hindrance between the close-contacted hydrogen atoms on acridinium and adjacent phenylene units (Fig. S76).

Photophysical properties

With the acridinium macrocycle in hand, we proceeded to investigate the photophysical properties of this compound together with its two precursor macrocycles (Fig. 3a and Table S1). The absorption spectra of **Ad[10]CPP-H** and **Ad[10]CPP-OH** were nearly identical, both exhibiting overlapping absorption

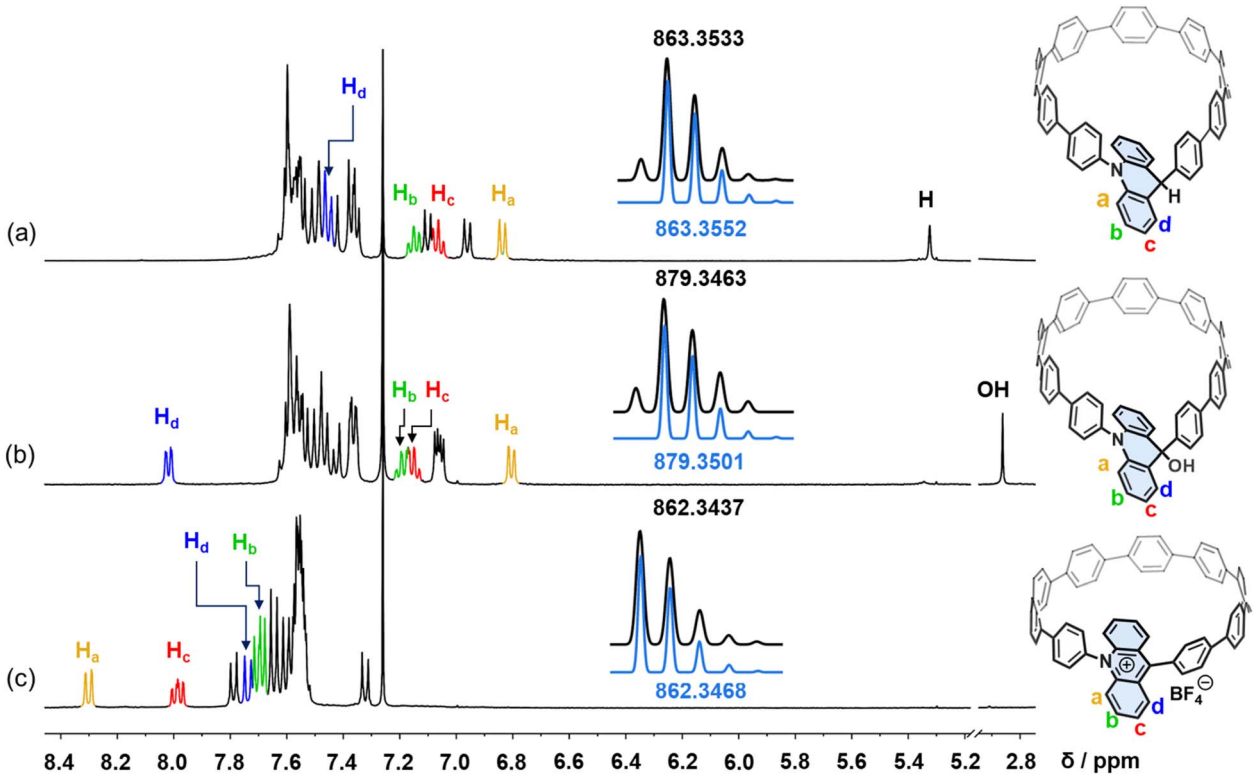

Fig. 2 Partial ^{1}H NMR spectra (400 MHz, $CDCl_3$, 298 K) of (a) **Ad[10]CPP-H**, (b) **Ad[10]CPP-OH**, and (c) **Ad[10]CPP-OH** upon addition of excess aqueous HBF_4 (40%). Insets show the experimental (black) and simulated (blue) MALDI-TOF-HRMS data for **Ad[10]CPP-H**, **Ad[10]CPP-OH**, and **Ad[10]CPP$^+$**.

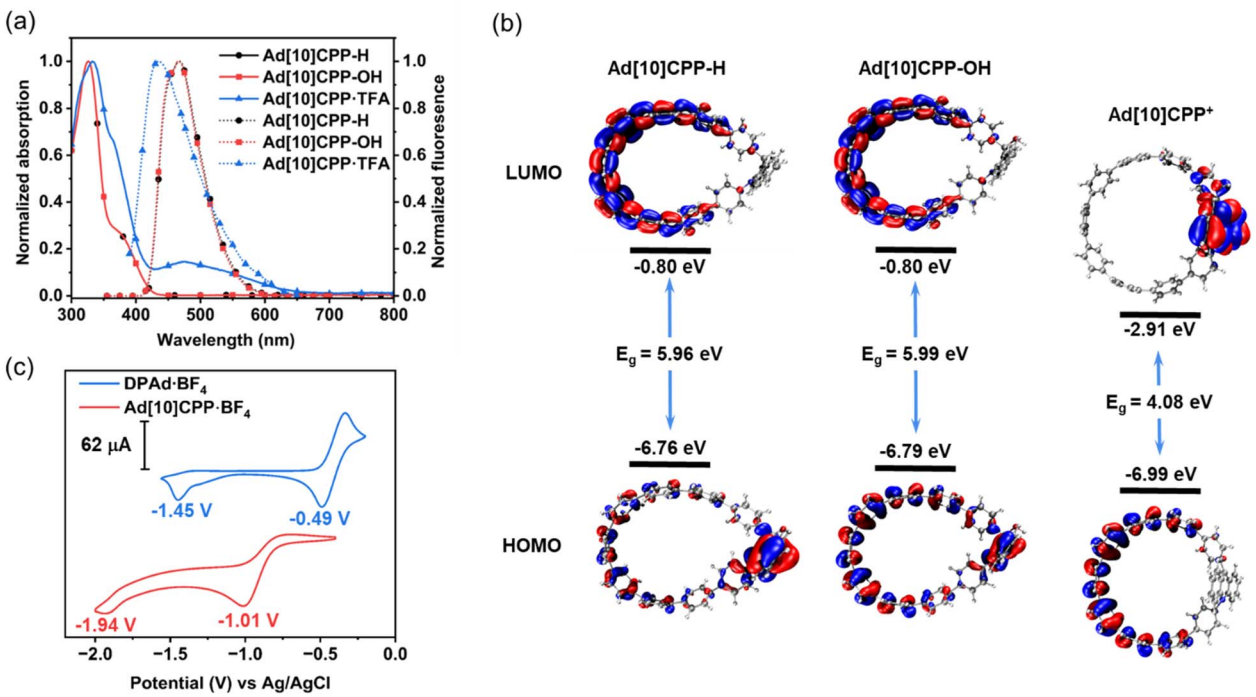

Fig. 3 (a) UV-vis absorption (solid line) and fluorescence emission (dotted line) spectra of **Ad[10]CPP-H** (λ_{ex} = 325 nm) (black circle), **Ad[10]CPP-OH** (λ_{ex} = 325 nm) (red square), and **Ad[10]CPP·TFA** (blue triangle) measured in CH_2Cl_2 solutions (1×10^{-5} M) at room temperature. The **Ad[10]CPP·TFA** sample is prepared by adding excess trifluoroacetic acid into **Ad[10]CPP-OH**, maintaining acid concentration at 1.0×10^{-3} M. (b) The DFT calculated frontier molecular orbitals and energy levels of **Ad[10]CPP-H**, **Ad[10]CPP-OH** and **Ad[10]CPP$^+$**. (c) CV of 1.0 mM DPAd·BF_4 in CH_2Cl_2 solution and **Ad[10]CPP·BF_4** in CH_3CN solution (Ag/AgCl, 0.1 M *n*-Bu_4NBF_4, 100 mV s^{-1}).

bands between 300 and 440 nm and lacking a broad charge-transfer band. Both compounds showed an absorption maximum (λ_{max}) at 326 nm, accompanied by a shoulder at approximately 378 nm. Time-dependent density functional theory (TD-DFT) calculations indicate that the major absorption at 326 nm arises from a combination of transitions: for **Ad[10]CPP-H**, these are HOMO−2 → LUMO, HOMO−1 → LUMO+1 and HOMO → LUMO+1 (Table S6); for **Ad[10]CPP-OH**, they are HOMO−2 → LUMO and HOMO → LUMO+1 (Table S7). In both **Ad[10]CPP-H** and **Ad[10]CPP-OH**, the HOMO is primarily confined to the oligoparaphenylene loop, indicating that the acridine segment acts as an electron donor in these neutral systems. A more pronounced spectroscopic change was observed upon protonating **Ad[10]CPP-OH** to form **Ad[10]CPP$^+$**. The absorption maximum λ_{max} of **Ad[10]CPP$^+$** was observed at 332 nm (Fig. 3a), which is slightly blue-shifted compared to **[10]CPP** (λ_{max} = 341 nm)[66] but red-shifted relative to **Ad[10]CPP-OH** (λ_{max} = 326 nm). The main absorption band of **Ad[10]CPP$^+$** is attributed to HOMO−1 → LUMO+1 and HOMO → LUMO+2 transitions (Table S8). Additionally, a shoulder peak appeared at around 365 nm, along with a broad characteristic charge-transfer band spanning from 420 nm to nearly 700 nm. TD-DFT calculations attribute this broad band to several transitions, including HOMO−4 → LUMO, HOMO−2 → LUMO, HOMO−1 → LUMO, and HOMO → LUMO. The frontier molecular orbital calculations further reveal that the HOMO of **Ad[10]CPP$^+$** is localized on the oligoparaphenylene loop, while the LUMO is confined to the acridinium unit and its adjacent aromatic rings (Fig. 3b). This distinct spatial separation of orbitals is characteristic of a donor–acceptor system. Compared to **Ad[10]CPP-OH**, the HOMO and LUMO energy levels of **Ad[10]CPP$^+$** are lowered by approximately 2.11 eV and 0.2 eV (Fig. 3b). This decrease in frontier molecular orbital energy is attributed to the formation of a rigid cationic framework and electron delocalization within the acridinium fragment, which significantly stabilizes the entire π-system, particularly the HOMO.

The fluorescence properties of **Ad[10]CPP-H** and **Ad[10]CPP-OH** were found to be similar. Both exhibited emission bands at nearly identical wavelengths (λ_{em} = 467 nm for **Ad[10]CPP-H** and 466 nm for **Ad[10]CPP-OH**; Fig. 3a) and high absolute fluorescence quantum yields (Φ_F = 70.9% for **Ad[10]CPP-H** and 67.3% for **Ad[10]CPP-OH**; Fig. S32 and S33). Their singlet excited-state lifetimes (τ) were measured *via* time-resolved fluorescence spectroscopy to be 2.48 ns for **Ad[10]CPP-H** and 2.40 ns for **Ad[10]CPP-OH**, respectively (Fig. S35 and S36). A pronounced change was observed upon protonation of **Ad[10]CPP-OH**. The gradual addition of TFA to **Ad[10]CPP-OH** led to significant fluorescence quenching, with emission nearly completely suppressed upon full conversion to **Ad[10]CPP$^+$** (Fig. S27). The cationic species **Ad[10]CPP$^+$** itself displayed very weak fluorescence with an emission maximum blue-shifted to 435 nm (Fig. 3a). This weak emission further decreased in intensity and underwent an additional blue shift as the concentration of TFA was further elevated (Fig. S28). The stability of **Ad[10]CPP$^+$** is contingent on excess acid, a condition that inevitably modifies its photophysical behavior, resulting in a pronounced acid concentration-dependent blue shift emission. This phenomenon likely arises because the acidic environment alters the excited-state decay pathway, potentially favoring radiative transition from a higher-energy localized excited (LE) state on the acridinium moiety (Fig. S30). The absolute fluorescence quantum yield of **Ad[10]CPP$^+$** was determined to be only 0.95% (Fig. S34) and the singlet excited-state lifetime was measured to be 1.88 ns (Fig. S37). Based on these values, the nonradiative decay rate constant ($k_{nr} = 5.3 \times 10^8\ s^{-1}$) is significantly higher than the radiative decay rate constant ($k_r = 5.1 \times 10^6\ s^{-1}$), indicating that the excited-state energy of **Ad[10]CPP$^+$** is primarily dissipated through non-radiative pathways. To gain further insight into the nature of the emissive state, we examined the emission spectra of **Ad[10]CPP$^+$** in solvents of varying polarity (CCl_4, $CHCl_3$, $C_2H_2Cl_4$, CH_2Cl_2, and $C_2H_4Cl_2$). A small negative solvatochromic effect of approximately 20 nm was observed (Fig. S29), suggesting that the emissive state is likely a LE state with only minor ICT character.[67,68] Several donor–acceptor cycloparaphenylene derivatives have been reported to exhibit low quantum yields due to significant spatial HOMO–LUMO separation that promotes non-radiative deactivation of the excited state.[34,35,69–77]

Electrochemical properties

The electrochemical behavior of **Ad[10]CPP$^+$** was elucidated through cyclic voltammetry (CV) and differential pulse voltammetry (DPV), with DPAd$^+$ serving as a comparative control (Fig. 3c, S41 and S42). The reference compound DPAd·BF_4 revealed two distinct reduction waves at −0.49 V and −1.45 V (*vs.* Ag/AgCl), respectively.[78] These waves correspond to two single-electron reduction processes, where DPAd·BF_4 first undergoes a reversible one-electron reduction to a radical species, followed by an irreversible one-electron reduction to form an anionic intermediate, which then captures a proton to afford DPAd-H (Fig. S38a).[79–81] **Ad[10]CPP·BF_4** displays similar two single-electron reduction processes with two notable distinctions. Firstly, the redox waves were shifted to a more negative potential by approximately 400 mV, appearing at −1.01 V and −1.94 V, respectively. Secondly, the transition to the radical state exhibited a semi-reversible nature (Fig. S38b). The calculated radical state **Ad[10]CPP$^\bullet$** shows a geometry between the teardrop shape of **Ad[10]CPP-H**/**Ad[10]CPP-OH** and the close-to-circle shape of **Ad[10]CPP$^+$**, namely, the ratio of the long axis and short axis of the radical state falls between them (Fig. S74). It is postulated that a geometrical change occurs upon the formation of the radical species, which, when attempting to revert the acridinium form, requires the molecular framework to overcome significant ring strain. In our subsequent efforts, we attempted to generate and characterize **Ad[10]CPP$^\bullet$**, the radical state of the macrocycle. As previously noted, the acridinium form **Ad[10]CPP$^+$** is only stable under moderately acidic conditions, which posed a challenge for generating radicals through reduction with active metals or cobaltocene, as these reagents tend to react with the acid first.

To circumvent this issue, we tried an alternative strategy involving the oxidation of **Ad[10]CPP-H** to achieve the radical state by treating **Ad[10]CPP-H** with nitrosonium

tetrafluoroborate ($NOBF_4$), a well-known one-electron oxidizing agent. To our surprise, **Ad[10]CPP-dimers** were generated after quenching the solution with air, as indicated in the HR-MS spectra (Fig. S24). This result suggests that the generated radical species is highly prone to dimerization. We were able to isolate the dimers. The ^{1}H NMR and ^{1}H–^{1}H COSY spectra (Fig. S52 and S53) indicated a mixture of two compounds in a ~7 : 3 ratio with very similar structures, as they were not differentiated by diffusion constants in the DOSY spectrum (Fig. S55) or the analytical HPLC trace (Fig. S56). This also explains the lack of hyperfine splitting patterns in the EPR spectrum (Fig. S47a). Further oxidizing the isolated dimers produces a broad near-infrared absorption band in the UV-vis-NIR spectrum ranging from 1000 nm to 2000 nm, with λ_{max} at 1574 nm (Fig. S58), possibly coming from diradical dications of the dimers.[82] A plausible mechanism for the formation of **Ad[10]CPP-dimers** is illustrated in Fig. S54. Oxidation of **Ad[10]CPP-H** generates a prochiral radical cation, which can dimerize by forming a new σ-bond at the *para* positions relative to the nitrogen atom. This process, accompanied by the loss of two protons, yields a *meso* dimer and a pair of racemic dimers. The inherent strain in **Ad[10]CPP-H** induces an electronic effect that governs a highly selective dimerization pathway, leading to the formation of giant double nanohoops.

Host and guest interactions

With the structure of **Ad[10]CPP$^+$** well characterized, we proceeded to evaluate its host capabilities for binding guest molecules, focusing on C_{60} due to the expected similarity in cavity size between **Ad[10]CPP$^+$** and **[10]CPP**.[45] Significant chemical shift changes in the ^{1}H NMR spectra of **Ad[10]CPP·TFA** upon the addition of C_{60} provided clear evidence of strong supramolecular interactions between the two species (Fig. S60). The binding constant of **Ad[10]CPP·TFA** and C_{60} was determined to be $(2.18 \pm 0.27) \times 10^4$ M^{-1} (Fig. S61) by NMR titration experiments, which is smaller than that of **[10]CPP**, $(2.79 \pm 0.03) \times 10^6$ M^{-1}, for C_{60} characterized by fluorescence-quenching experiments.[44]

After multiple attempts, we successfully obtained single crystals of the host–guest complex **C_{60}⊂Ad[10]CPP·TFA** suitable for X-ray diffraction analysis. The crystal structure unambiguously confirms a 1 : 1 host–guest complex, with the C_{60} guest residing within the cavity of **Ad[10]CPP·TFA** (Fig. 4). The cycloparaphenylene host exhibits a slightly elliptical shape, with a long and short axis of 14.0 Å and 13.6 Å, respectively (Fig. 4a and b). Further structural analysis reveals more compact supramolecular interactions compared to **C_{60}⊂[10]CPP**, as evidenced by the shorter average distance (3.21 Å) from the equatorial carbon atoms of C_{60} to the nearest phenylene plane of the host, relative to the 3.44 Å observed in the latter[45] (Fig. S71). The torsion angles between the acridinium and its adjacent phenylene moieties are 53.8° and 75.8°, respectively, markedly larger than those between other phenylene rings (8.3°–29.0°), which can be attributed to steric repulsion from the hydrogen atoms at the acridinium–phenylene junctions (Fig. S72). Additionally, the acridinium fragment forms

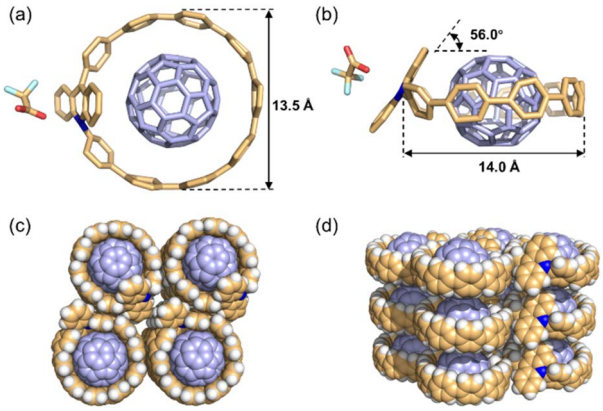

Fig. 4 (a) Top view and (b) side view of the X-ray solid-state structure of C_{60}⊂Ad[10]CPP·TFA. Hydrogen atoms are omitted for clarity. (c) Top view and (d) side view of crystal packing showing columnar stacks of C_{60}⊂Ad[10]CPP·TFA; solvent molecules and counterions are omitted for clarity. Color code: C, tan/lavender; N, blue; O, red; F, pale cyan. For crystallographic details and CCDC numbers see the SI.

a dihedral angle of 57.2° with the macrocyclic plane (Fig. 4b). Collectively, we propose that this strained, elliptical structure imposes a certain compression upon C_{60} encapsulation, which diminishes the optimal host–guest complementarity achieved in the nearly circular **[10]CPP** complex, thereby accounting for the lower binding constant.

In order to assess the stabilizing effect of C_{60} encapsulation on the **Ad[10]CPP$^+$** host, we conducted systematic titration experiments using TFA. The protonation processes of **Ad[10]CPP-OH** by TFA were monitored *via* characteristic NMR signals, both in the presence and absence of C_{60} (Fig. S62 and S63). A change in solvent (CH_2Cl_2 to $C_2Cl_4D_2$) lowered the concentration of TFA required for the complete conversion of **Ad[10]CPP-OH** to **Ad[10]CPP$^+$**. At a TFA concentration of 1.0×10^{-4} M, the conversion of free **Ad[10]CPP-OH** was negligible, whereas partial conversion was achieved when C_{60} was present. This stabilization effect was further confirmed at a TFA concentration of 2.0×10^{-4} M, where **Ad[10]CPP-OH** alone underwent incomplete conversion, but full conversion was achieved in the presence of excess C_{60} (Fig. S64 and S65). These results demonstrate that host–guest complexation stabilizes the vulnerable structure of the host, thereby reducing the acid requirement for stabilizing the cationic host structure. This provides direct evidence that C_{60} substantially reinforces the molecular scaffold *via* π–π interactions. The encapsulation improves its stability against atmospheric moisture compared to the empty host, enabling the successful growth of single crystals suitable for X-ray diffraction, ultimately allowing us to resolve the structure of the **C_{60}⊂Ad[10]CPP·TFA** complex.

Stimulus responsive system

With the binding affinity between **Ad[10]CPP·TFA** and C_{60} measured and the structure of host–guest complex characterized, we then explored the acid–base stimuli responsive properties of the host–guest complex (Fig. 5a). Gradually adding five

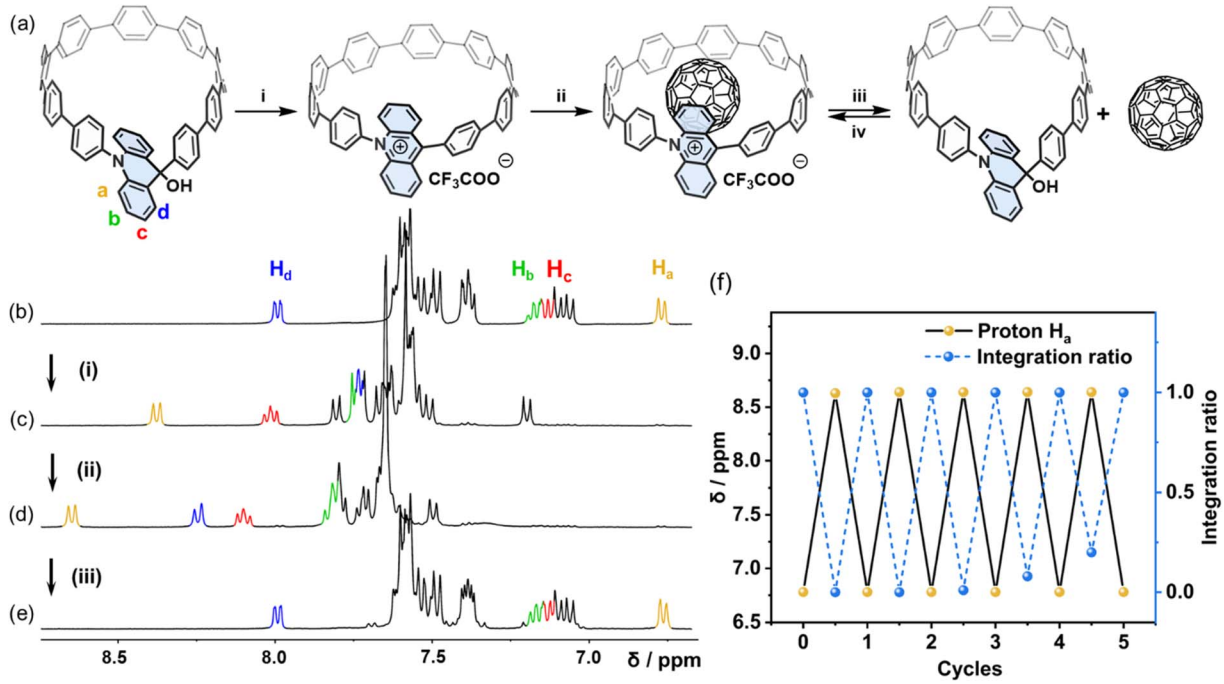

Fig. 5 (a) Schematic representation of acid–base responsive capture and release of C_{60} (0–4.09 mM) by macrocycle **Ad[10]CPP·TFA** (0.53 mM) in CD_2Cl_2. Conditions and reagents: (i) TFA, CD_2Cl_2, (ii) C_{60}, CD_2Cl_2, ultrasound, and (iii) TEA, CD_2Cl_2, (iv) TFA, CD_2Cl_2, ultrasound. ^{1}H NMR spectra (400 MHz, CD_2Cl_2, 298 K) of (b) **Ad[10]CPP-OH** and with sequential addition of (c) 5 eq. of TFA, (d) 1.5 eq. of C_{60}, and (e) 5 eq. of TEA. (f) Capture and release of C_{60} cycles of **Ad[10]CPP·TFA** under acid/neutral conditions, monitored using the ^{1}H NMR spectra.

equivalents of TFA to an NMR tube containing a CD_2Cl_2 solution of **Ad[10]CPP-OH** (Fig. 5b) caused a significant chemical shift change in the proton associated with the acridinium moiety. Specifically, H_a shifted from 6.78 ppm to 8.37 ppm, indicating complete transformation into **Ad[10]CPP·TFA** (Fig. 5c). Subsequently, adding 1.5 equivalents of C_{60} to the same NMR tube caused H_a to shift further downfield to 8.64 ppm, attributed to the formation of the host–guest complex **C_{60}⊂Ad[10]CPP·TFA** (Fig. 5d). Adding five equivalents of triethylamine (TEA) to the solution caused the H_a signal to revert to 6.78 ppm, indicating that the macrocycle had completely transformed back into **Ad[10]CPP-OH** (Fig. 5e). Since the cavity of **Ad[10]CPP-OH** is not suitable for C_{60} (Fig. S59), the guest molecule is then released into the solution. The acid–base switch process is reversible for at least 5 cycles, as monitored by ^{1}H NMR spectroscopy (Fig. 5f and S67).

Conclusions

In summary, we successfully synthesized and characterized an acridinium-functionalized cycloparaphenylene derivative, **Ad[10]CPP$^+$**. Structural characterization indicates that **Ad[10]CPP$^+$** adopts a nearly circular configuration similar to **[10]CPP**, with increased torsion angles in the acridinium moiety due to steric hindrance. Electrochemical studies reveal two well-separated reduction peaks for **Ad[10]CPP$^+$**, suggesting its potential to form a radical species, **Ad[10]CPP$^\bullet$**. However, attempts to generate **Ad[10]CPP$^\bullet$** through oxidation resulted in its dimerization, yielding giant double nanohoops. **Ad[10]CPP$^+$** also demonstrates strong host–guest interactions with electron-rich fullerenes, as evidenced by NMR spectroscopy and single-crystal X-ray analysis. Furthermore, **Ad[10]CPP$^+$** can undergo reversible structural transformations in response to chemical stimuli, enabling controlled capture and release of fullerene guests under alternating acidic and basic conditions for multiple cycles. The acid–base triggered guest capture and release of **Ad[10]CPP$^+$** represents a valuable addition to the cycloparaphenylene family. Its key advantage lies in the highly confined cavity and switchable cationic character. Our current efforts are focused on leveraging multi-acridinium motifs to develop advanced functional systems for applications in sensing wider guests.

Author contributions

C. C. conceived and supervised the project. J. M. performed most of the synthesis and characterization experiments. J. Z. and P. Y. conducted the calculations. Y. H., J. J., X. Z. and H. Z. helped with synthesis of starting materials. K. L., D. Z., and P. L. helped with characterization. All authors contributed to manuscript writing.

Conflicts of interest

There are no conflicts to declare.

Data availability

CCDC 2449558, 2449559 and 2449561 contain the supplementary crystallographic data for this paper.[83a–c]

Supplementary information (SI): additional experimental details, materials and methods, ^{1}H and ^{13}C NMR, (^{1}H, ^{1}H)-COSY NMR, MS, and UV-vis-IR spectra, EPR spectra, crystallographic data, and computational details (PDF). See DOI: https://doi.org/10.1039/d6sc01132b.

Acknowledgements

This work was supported by the Fundamental Research Funds for the Central Universities and NSFC 22171193. We thank Professor Lihua Yuan and Professor Xiaowei Li at Sichuan University for their help with UV-vis and fluorescence spectroscopy. We thank Yuxuan He, Professor Zhengyang Bin and Professor Jinsong You at Sichuan University for their help with the measurement of lifetimes of the singlet excited states and the fluorescence quantum yield. We thank Yimeng Hu, Professor Liangfang Zhu and Professor Changwei Hu at Sichuan University for UV-Vis-NIR spectroscopy. We thank Lingyan Sun and Professor Cheng Zhang at Sichuan University for their help with HPLC chromatograms. We thank Dr Jing Li, Dr Chunxia Wang and Dr Dongyan Deng from Sichuan University for HR-MS and NMR testing, respectively. We thank Dr Fucheng Leng at Westlake University for the single-crystal crystallography. Computational work was supported by the Center for Computational Science and Engineering and the CHEM High-Performance Supercomputer Cluster (CHEM-HPC) of the Department of Chemistry, Southern University of Science and Technology.

References

1 R. Jasti, J. Bhattacharjee, J. B. Neaton and C. R. Bertozzi, Synthesis, Characterization, and Theory of [9]-, [12]-, and [18]Cycloparaphenylene: Carbon Nanohoop Structures, *J. Am. Chem. Soc.*, 2008, **130**, 17646–17647.

2 S. E. Lewis, Cycloparaphenylenes and related nanohoops, *Chem. Soc. Rev.*, 2015, **44**, 2221–2304.

3 Y. Segawa, A. Yagi, K. Matsui and K. Itami, Design and Synthesis of Carbon Nanotube Segments, *Angew. Chem., Int. Ed.*, 2016, **55**, 5136–5158.

4 Y. Xu and M. von Delius, The Supramolecular Chemistry of Strained Carbon Nanohoops, *Angew. Chem., Int. Ed.*, 2020, **59**, 559–573.

5 J. Wang, X. Zhang, H. Jia, S. Wang and P. Du, Large π-Extended and Curved Carbon Nanorings as Carbon Nanotube Segments, *Acc. Chem. Res.*, 2021, **54**, 4178–4190.

6 Y. Li, H. Kono, T. Maekawa, Y. Segawa, A. Yagi and K. Itami, Chemical Synthesis of Carbon Nanorings and Nanobelts, *Acc. Mater. Res.*, 2021, **2**, 681–691.

7 X. Li, S. Guo and H. Jiang, Recent advances in functionalized cycloparaphenylenes: from molecular design to applications, *Chem. Commun.*, 2025, **61**, 9836–9852.

8 M. Hermann, D. Wassy and B. Esser, Conjugated Nanohoops Incorporating Donor, Acceptor, Hetero- or Polycyclic Aromatics, *Angew. Chem., Int. Ed.*, 2021, **60**, 15743–15766.

9 E. Kayahara, R. Qu and S. Yamago, Bromination of Cycloparaphenylenes: Strain-Induced Site-Selective Bis-Addition and Its Application for Late-Stage Functionalization, *Angew. Chem., Int. Ed.*, 2017, **56**, 10428–10432.

10 E. Kayahara, T. Hayashi, K. Takeuchi, F. Ozawa, K. Ashida, S. Ogoshi and S. Yamago, Strain-Induced Double Carbon–Carbon Bond Activations of Cycloparaphenylenes by a Platinum Complex: Application to the Synthesis of Cyclic Diketones, *Angew. Chem., Int. Ed.*, 2018, **57**, 11418–11421.

11 T. Terabayashi, E. Kayahara, Y. Zhang, Y. Mizuhata, N. Tokitoh, T. Nishinaga, T. Kato and S. Yamago, Synthesis of Twisted [n]Cycloparaphenylene by Alkene Insertion, *Angew. Chem., Int. Ed.*, 2023, **62**, e202214960.

12 J. M. Fehr, N. Myrthil, A. L. Garrison, T. W. Price, S. A. Lopez and R. Jasti, Experimental and theoretical elucidation of SPAAC kinetics for strained alkyne-containing cycloparaphenylenes, *Chem. Sci.*, 2023, **14**, 2839–2848.

13 T. D. Clayton, J. M. Fehr, T. W. Price, L. N. Zakharov and R. Jasti, Pinwheel-like Curved Aromatics from the Cyclotrimerization of Strained Alkyne Cycloparaphenylenes, *J. Am. Chem. Soc.*, 2024, **146**, 30607–30614.

14 K. Lan, C. Zhang, Y. Li, C. Hu, Z. Su and C. Cheng, Strain Energy Prompted Tunable Aggregation-Induced Emission Property of Tetraphenylethylene, *Angew. Chem., Int. Ed.*, 2025, **64**, e202507763.

15 K. Lan, S. Zhang, Y. Lu, P. Yu, J. Chen and C. Cheng, Strain Energy Induced Rotary Speed Acceleration in a Light- Driven Molecular Motor, *Angew. Chem., Int. Ed.*, 2025, **64**, e202507487.

16 Z. A. Huang, C. Chen, X. D. Yang, X. B. Fan, W. Zhou, C. H. Tung, L. Z. Wu and H. Cong, Synthesis of Oligoparaphenylene-Derived Nanohoops Employing an Anthracene Photodimerization-Cycloreversion Strategy, *J. Am. Chem. Soc.*, 2016, **138**, 11144–11147.

17 Y. Segawa, M. Kuwayama and K. Itami, Synthesis and Structure of [9]Cycloparaphenylene Catenane: An All-Benzene Catenane Consisting of Small Rings, *Org. Lett.*, 2020, **22**, 1067–1070.

18 K. Li, S. Yoshida, R. Yakushiji, X. Liu, C. Ge, Z. Xu, Y. Ni, X. Ma, J. Wu, S. Sato and Z. Sun, Molecular cylinders with donor–acceptor structure and swinging motion, *Chem. Sci.*, 2024, **15**, 18832–18839.

19 G. Li, X. Wang, L. L. Mao, J. N. Gao, X. Shi, H. Li, Z. T. Li, Z. Y. Huo, Y. Chen, H. B. Yang, J. Chen, C. H. Tung, L. Z. Wu and H. Cong, Tubular All-Benzene Nanocarbon with Evolving Excited-State Chirality, *Angew. Chem., Int. Ed.*, 2025, e202518587.

20 W. Shi, Y. Hu, L. Leanza, Y. Shchukin, P. A. Hoffmann, M.-H. Li, C. Ning, Z.-Y. Cao, Y.-Q. Xu, P. Du, M. von Delius, G. M. Pavan and Y. Xu, Ring-in-Ring Assembly Facilitates the Synthesis of a [12]Cycloparaphenylene ABC-Type [3] Catenane, *Angew. Chem., Int. Ed.*, 2025, **64**, e202421459.

21 L. Zhan, C. Dai, G. Zhang, J. Zhu, S. Zhang, H. Wang, Y. Zeng, C. H. Tung, L. Z. Wu and H. Cong, A Conjugated Figure-of-Eight Oligoparaphenylene Nanohoop with Adaptive Cavities Derived from Cyclooctatetrathiophene Core, *Angew. Chem., Int. Ed.*, 2022, **61**, e202113334.

22 P. Fang, M. Chen, N. Yin, G. Zhuang, T. Chen, X. Zhang and P. Du, Regulating supramolecular interactions in dimeric macrocycles, *Chem. Sci.*, 2023, **14**, 5425–5430.
23 A. A. Kamin, T. D. Clayton, C. E. Otteson, P. M. Gannon, S. Krajewski, W. Kaminsky, R. Jasti and D. J. Xiao, Synthesis and metalation of polycatechol nanohoops derived from fluorocycloparaphenylenes, *Chem. Sci.*, 2023, **14**, 9724–9732.
24 M. S. Mirzaei, S. Mirzaei, V. M. Espinoza Castro, C. Lawrence and R. Hernández Sánchez, Dual molecular tweezers extending from a nanohoop, *Chem. Commun.*, 2024, **60**, 14236–14239.
25 K. Kovida, J. Malinčík, C. M. Cruz, A. G. Campaña and T. Šolomek, Role of exciton delocalization in chiroptical properties of benzothiadiazole carbon nanohoops, *Chem. Sci.*, 2025, **16**, 1405–1410.
26 Y. Hu, T. Li, T. Su, W. Shi, Y. Yu, B. Li, M.-H. Li, S. Zhang, Y.-Q. Xu, Q. Liu, D. Wu and Y. Xu, Crown ether–cycloparaphenylene hybrid multimacrocycles: insights into supramolecular gas sensing and biological potential, *Chem. Sci.*, 2025, **16**, 13115–13121.
27 T. Kato, D. Imoto, A. Yagi and K. Itami, Making non-emissive [6]cycloparaphenylene fluorescent by simple multiple methyl substitution, *Chem. Sci.*, 2025, **16**, 18952–18958.
28 N. Liu, Y. Choi, Z. Zong, T. Feng, T. Kim and X.-S. Ke, BODIPY-Cycloparaphenylene Nanorings, *CCS Chem.*, 2025, **7**, 3650–3663.
29 M. Katsuma, S. Yasutomo and I. Kenichiro, Synthesis and Properties of Cycloparaphenylene-2,5-pyridylidene: A Nitrogen-Containing Carbon Nanoring, *Org. Lett.*, 2012, **14**, 1888–1891.
30 J. M. Van Raden, S. Louie, L. N. Zakharov and R. Jasti, 2,2'-Bipyridyl-Embedded Cycloparaphenylenes as a General Strategy To Investigate Nanohoop-Based Coordination Complexes, *J. Am. Chem. Soc.*, 2017, **139**, 2936–2939.
31 Y. Y. Fan, D. Chen, Z. A. Huang, J. Zhu, C. H. Tung, L. Z. Wu and H. Cong, An isolable catenane consisting of two Mobius conjugated nanohoops, *Nat. Commun.*, 2018, **9**, 3037.
32 J. H. May, J. M. Van Raden, R. L. Maust, L. N. Zakharov and R. Jasti, Active template strategy for the preparation of π-conjugated interlocked nanocarbons, *Nat. Chem.*, 2023, **15**, 170–176.
33 J. H. May, J. M. Fehr, J. C. Lorenz, L. N. Zakharov and R. Jasti, A High-Yielding Active Template Click Reaction (AT−CuAAC) for the Synthesis of Mechanically Interlocked Nanohoops, *Angew. Chem., Int. Ed.*, 2024, **63**, e202401823.
34 E. R. Darzi, E. S. Hirst, C. D. Weber, L. N. Zakharov, M. C. Lonergan and R. Jasti, Synthesis, Properties, and Design Principles of Donor-Acceptor Nanohoops, *ACS Cent. Sci.*, 2015, **1**, 335–342.
35 J. M. Van Raden, E. R. Darzi, L. N. Zakharov and R. Jasti, Synthesis and characterization of a highly strained donor-acceptor nanohoop, *Org. Biomol. Chem.*, 2016, **14**, 5721–5727.
36 T. Drennhaus, D. Imoto, E. S. Horst, L. Lezius, H. Shudo, T. Kato, K. Bergander, C. G. Daniliuc, D. Leifert, A. Yagi, A. Studer and K. Itami, Cycloparaazine, a full-azine carbon nanoring, *Nat. Commun.*, 2025, **16**, 4643.
37 T. Wu, J. Yang, Y. Liu, C. Wang, J. Zhang, R.-H. Zheng, H. Yu, R. Liu and D. Lu, Size-controlled synthesis of N-doped [10]CPPs and investigation on the variations of their binding affinities with fullerene, *Chin. Chem. Lett.*, 2025, 112199.
38 S. Qiu, Y. Zhao, L. Zhang, Y. Ni, Y. Wu, H. Cong, D.-H. Qu, W. Jiang, J. Wu, H. Tian and Z. Wang, Axially N-Embedded Quasi-Carbon Nanohoops with Multioxidation States, *CCS Chem.*, 2023, **5**, 1763–1772.
39 X. Zhang, J. Jiang, K. Lan, D. Zhang and C. Cheng, Cycloparaphenylene-Type Hoops with Adaptive Cavities Derived from N,N'-diphenyldihydrodibenzo[a,c]phenazine, *Org. Lett.*, 2025, **27**, 10484–10488.
40 R. Frydrych, K. Senthilkumar, K. Ślusarek, M. Waliczek, W. Bury, P. J. Chmielewski, J. Cybińska and M. Stępień, Viologen–cycloparaphenylene hybrids: luminescent molecular nanocarbons for anion binding and specific vapor sorption, *Org. Chem. Front.*, 2025, **12**, 437–447.
41 S. Qiu, L. Zhang, D.-H. Qu and Z. Wang, Supercycloalkanes: dihydropyrazine-embedded macrocycles with flexible conformations resembling cycloalkanes, *Chem. Sci.*, 2025, **16**, 20464–20472.
42 L. Zhang, S. Qiu, S. Hu, H. Xu, X. Sun, W. Jiang, D.-H. Qu and Z. Wang, Cocrystals of axially N-embedded quasi-carbon nanohoops via modulating the electron affinity of guest acceptors, *Sci. China Chem.*, 2025, **68**, 3154–3161.
43 D. Zhang, J. Liu, J. Ming, K. Lan, J. Jiang, H. Zhong, X. Zhang, Z. Bin and C. Cheng, Incorporating a Pyridinium into a Cycloparaphenylene: A Cati-onic Donor–Acceptor Nanohoop with Reversible Redox Properties, *Sci. China Chem.*, 2026, DOI: 10.1007/s11426-11025-13313-11429.
44 T. Iwamoto, Y. Watanabe, T. Sadahiro, T. Haino and S. Yamago, Size-Selective Encapsulation of C_{60} by [10]Cycloparaphenylene: Formation of the Shortest Fullerene-Peapod, *Angew. Chem., Int. Ed.*, 2011, **50**, 8342–8344.
45 J. Xia, J. W. Bacon and R. Jasti, Gram-scale synthesis and crystal structures of [8]- and [10]CPP, and the solid-state structure of C_{60}@[10]CPP, *Chem. Sci.*, 2012, **3**, 3018–3021.
46 T. Iwamoto, Y. Watanabe, H. Takaya, T. Haino, N. Yasuda and S. Yamago, Size- and Orientation- Selective Encapsulation of C_{70} by Cycloparaphenylenes, *Chem.–Eur. J.*, 2013, **19**, 14061–14068.
47 A. Stergiou, J. Rio, J. H. Griwatz, D. Arcon, H. A. Wegner, C. P. Ewels and N. Tagmatarchis, A Long-Lived Azafullerenyl Radical Stabilized by Supramolecular Shielding with a [10]Cycloparaphenylene, *Angew. Chem., Int. Ed.*, 2019, **58**, 17745–17750.
48 S. Wang, X. Li, X. Zhang, P. Huang, P. Fang, J. Wang, S. Yang, K. Wu and P. Du, A supramolecular polymeric heterojunction composed of an all-carbon conjugated polymer and fullerenes, *Chem. Sci.*, 2021, **12**, 10506–10513.
49 E. Ubasart, O. Borodin, C. Fuertes-Espinosa, Y. Xu, C. García-Simón, L. Gómez, J. Juanhuix, F. Gándara, I. Imaz, D. Maspoch, M. von Delius and X. Ribas, A three-shell supramolecular complex enables the symmetry-

mismatched chemo- and regioselective bis-functionalization of C_{60}, *Nat. Chem.*, 2021, **13**, 420–427.

50 Y. Xu, F. Steudel, M. Y. Leung, B. Xia, M. von Delius and V. W. W. Yam, [n]Cycloparaphenylene- Pillar[5]arene Bismacrocycles: Their Circularly Polarized Luminescence and Multiple Guest Recognition Properties, *Angew. Chem., Int. Ed.*, 2023, **62**, e202302978.

51 P. J. Evans, L. N. Zakharov and R. Jasti, Synthesis of carbon nanohoops containing thermally stable cis azobenzene, *J. Photochem. Photobiol., A*, 2019, **382**, 111878.

52 X. Li, L. Jia, W. Wang, Y. Wang, D. Sun and H. Jiang, A nonalternant azulene-embedded carbon nanohoop featuring anti-Kasha emission and tunable properties upon pH stimuli-responsiveness, *J. Mater. Chem. C*, 2023, **11**, 1429–1434.

53 T. Ide, W.-C. Huang and M. Horie, Tris-Azo Triangular Paraphenylenes: Synthesis and Reversible Interconversion into Radial π-Conjugated Macrocycles, *J. Am. Chem. Soc.*, 2024, **146**, 10246–10250.

54 S. Wu, J. Jie, L. Liu, L. Liu, S. Guo, X. Li, J. He, Z. Lian, Y. Wang, X. Xu, H. Su, X. Chen and H. Jiang, A Redox-Active π-Extended Tetrathiafulvalene-Based Carbon Nanohoop Featuring Unique Kasha/Anti-Kasha Dual Emissions: Structure, Photophysical Properties, and Photoconductivity, *Angew. Chem., Int. Ed.*, 2025, **64**, e202512167.

55 K. Kurihara, K. Yazaki, M. Akita and M. Yoshizawa, A Switchable Open/closed Polyaromatic Macrocycle that Shows Reversible Binding of Long Hydrophilic Molecules, *Angew. Chem., Int. Ed.*, 2017, **56**, 11360–11364.

56 J. Hu, J. S. Ward, A. Chaumont, K. Rissanen, J. M. Vincent, V. Heitz and H. P. Jacquot de Rouville, A Bis-Acridinium Macrocycle as Multi-Responsive Receptor and Selective Phase-Transfer Agent of Perylene, *Angew. Chem., Int. Ed.*, 2020, **59**, 23206–23212.

57 I. A. MacKenzie, L. Wang, N. P. R. Onuska, O. F. Williams, K. Begam, A. M. Moran, B. D. Dunietz and D. A. Nicewicz, Discovery and characterization of an acridine radical photoreductant, *Nature*, 2020, **580**, 76–80.

58 H. P. Jacquot de Rouville, J. Hu and V. Heitz, N-Substituted Acridinium as a Multi-Responsive Recognition Unit in Supramolecular Chemistry, *ChemPlusChem*, 2021, **86**, 110–129.

59 H.-P. Jacquot de Rouville, C. Gourlaouen, D. Bardelang, N. Le Breton, J. S. Ward, L. Ruhlmann, J.-M. Vincent, D. Jardel, K. Rissanen, J.-L. Clément, S. Choua and V. Heitz, Viridium: A Stable Radical and Its π-Dimerization, *J. Am. Chem. Soc.*, 2024, **147**, 1823–1830.

60 S. Claude, J.-M. Lehn, F. Schmidt and J.-P. Vigneron, Binding of Nucleosides, Nucleotides and Anionic Planar Substrates by Bis-lntercaland Receptor Molecules, *J. Chem. Soc., Chem. Commun.*, 1991, 1182–1185.

61 H. Kawai, T. Takeda, K. Fujiwara, M. Wakeshima, Y. Hinatsu and T. Suzuki, Ultralong Carbon–Carbon Bonds in Dispirobis(10-methylacridan) Derivatives with an Acenaphthene, Pyracene, or Dihydropyracylene Skeleton, *Chem.–Eur. J.*, 2008, **14**, 5780–5793.

62 A. Petitjean, R. G. Khoury, N. Kyritsakas and J.-M. Lehn, Dynamic Devices. Shape Switching and Substrate Binding in Ion-Controlled Nanomechanical Molecular Tweezers, *J. Am. Chem. Soc.*, 2004, **126**, 6637–6647.

63 W. Abraham, K. Buck, M. Orda-Zgadzaj, S. Schmidt-Schäffer and U.-W. Grummt, Novel photoswitchable rotaxanes, *Chem. Commun.*, 2007, 3094–3096.

64 X. Zhang, K. Lan and C. Cheng, Figure-Eight Bismacrocycles Derived from a Tetraphenylmethane Core and Oligoparaphenylene Loops, *Org. Lett.*, 2024, **26**, 7853–7857.

65 V. K. Patel, E. Kayahara and S. Yamago, Practical Synthesis of [n]Cycloparaphenylenes (n=5, 7-12) by H_2SnCl_4-Mediated Aromatization of 1,4-Dihydroxycyclo-2,5-diene Precursors, *Chem.–Eur. J.*, 2015, **21**, 5742–5749.

66 T. Iwamoto, Y. Watanabe, Y. Sakamoto, T. Suzuki and S. Yamago, Selective and Random Syntheses of [n] Cycloparaphenylenes (n = 8-13) and Size Dependence of Their Electronic Properties, *J. Am. Chem. Soc.*, 2011, **133**, 8354–8361.

67 B. Carlotti, A. Cesaretti, C. G. Fortuna, A. Spalletti and F. Elisei, Experimental evidence of dual emission in a negatively solvatochromic push–pull pyridinium derivative, *Phys. Chem. Chem. Phys.*, 2015, **17**, 1877–1882.

68 P. Sumsalee, P. Morgante, G. Pieters, J. Crassous, J. Autschbach and L. Favereau, Negative solvatochromism and sign inversion of circularly polarized luminescence in chiral exciplexes as a function of solvent polarity, *J. Mater. Chem. C*, 2023, **11**, 8514–8523.

69 T. Kuwabara, J. Orii, Y. Segawa and K. Itami, Curved Oligophenylenes as Donors in Shape-Persistent Donor-Acceptor Macrocycles with Solvatofluorochromic Properties, *Angew. Chem., Int. Ed.*, 2015, **54**, 9646–9649.

70 T. C. Lovell, Z. R. Garrison and R. Jasti, Synthesis, Characterization, and Computational Investigation of Bright Orange-Emitting Benzothiadiazole [10] Cycloparaphenylene, *Angew. Chem., Int. Ed.*, 2020, **59**, 14363–14367.

71 D. Chen, Y. Wada, Y. Kusakabe, L. Sun, E. Kayahara, K. Suzuki, H. Tanaka, S. Yamago, H. Kaji and E. Zysman-Colman, A Donor-Acceptor 10-Cycloparaphenylene and Its Use as an Emitter in an Organic Light-Emitting Diode, *Org. Lett.*, 2023, **25**, 998–1002.

72 V. Bliksted Roug Pedersen, T. W. Price, N. Kofod, L. N. Zakharov, B. W. Laursen, R. Jasti and M. Brøndsted Nielsen, Synthesis and Properties of Fluorenone-Containing Cycloparaphenylenes and Their Late-Stage Transformation, *Chem.–Eur. J.*, 2023, **30**, e202303490.

73 P. Fang, Z. Cheng, W. Peng, J. Xu, X. Zhang, F. Zhang, G. Zhuang and P. Du, A Strained Donor-Acceptor Carbon Nanohoop: Synthesis, Photophysical and Charge Transport Properties, *Angew. Chem., Int. Ed.*, 2024, **63**, e202407078.

74 C. Brouillac, E. Dureau, O. Jeannin, J. Rault-Berthelot, C. Poriel and C. Quinton, Donor–Acceptor Nanohoops: Impact of the Ratio and Arrangement of the Fluorenone and Carbazole Moieties, *J. Am. Chem. Soc.*, 2025, **147**, 11267–11276.

75 S. Guo, L. Liu, L. Liu, Y. Fan, H. Yang, J. He, Y. Wang, Z. Bo, X. Xu, X. Chen and H. Jiang, Naphthalene Diimide-Embedded Donor-Acceptor Carbon Nanohoops: Photophysical, Photoconductive, and Charge Transport Properties, *ACS Appl. Mater. Interfaces*, 2025, **17**, 5202–5212.
76 X. Li, L. Liu, L. Jia, Z. Lian, J. He, S. Guo, Y. Wang, X. Chen and H. Jiang, Acceptor engineering of quinone-based cycloparaphenylenes via post-synthesis for achieving white-light emission in single-molecule, *Nat. Commun.*, 2025, **16**, 467.
77 T. C. Lovell, K. G. Fosnacht, C. E. Colwell and R. Jasti, Effect of curvature and placement of donor and acceptor units in cycloparaphenylenes: a computational study, *Chem. Sci.*, 2020, **11**, 12029–12035.
78 T. P. Vaid, A. K. Lytton-Jean and B. C. Barnes, Investigations of the 9,10-Diphenylacridyl Radical as an Isostructural Dopant for the Molecular Semiconductor 9,10-Diphenylanthracene, *Chem. Mater.*, 2003, **15**, 4292–4299.
79 P. Hapiot, J. Moiroux and J.-M. Savéant, Electrochemistry of NADH/NAD+ Analogues. A Detailed Mechanistic Kinetic and Thermodynamic Analysis of the 10-Methylacridan/10-Methylacridinium Couple in Acetonitrile, *J. Am. Chem. Soc.*, 1990, **112**, 1337–1343.
80 D. T. Hogan and T. C. Sutherland, Modern Spin on the Electrochemical Persistence of Heteroatom-Bridged Triphenylmethyl-Type Radicals, *J. Phys. Chem. Lett.*, 2018, **9**, 2825–2829.
81 S. A. Jonker, F. Ariese and J. W. Verhoeven, Cation complexation with functionalized 9-arylacridinium ions: Possible applications in the development of cation-selective optical probes, *Recl. Trav. Chim. Pays-Bas*, 1989, **108**, 109–115.
82 K. Kamada, S.-i. Fuku-en, S. Minamide, K. Ohta, R. Kishi, M. Nakano, H. Matsuzaki, H. Okamoto, H. Higashikawa, K. Inoue, S. Kojima and Y. Yamamoto, Impact of Diradical Character on Two-Photon Absorption: Bis(acridine) Dimers Synthesized from an Allenic Precursor, *J. Am. Chem. Soc.*, 2012, **135**, 232–241.
83 (*a*) CCDC 2449558: Experimental Crystal Structure Determination, 2026, DOI: 10.5517/ccdc.csd.cc2n6z0w; (*b*) CCDC 2449559: Experimental Crystal Structure Determination, 2026, DOI: 10.5517/ccdc.csd.cc2n6z1x; (*c*) CCDC 2449561: Experimental Crystal Structure Determination, 2026, DOI: 10.5517/ccdc.csd.cc2n6z3z.